Influence of Internal Stress Coupling on the Deformation Behavior of NiTi-Nb Nanowire Composites

Zhenyang Liu[1], Lishan Cui[1]*, Yinong Liu[2], Daqiang Jiang[1], Jiang Jiang[1], Xiaobin Shi[1], Yang Shao[1], Yanjun Zheng[1]

1Department of Materials Science and Engineering, China University of Petroleum-Beijing, Beijing 102249 China
2School of Mechanical and Chemical Engineering, The University of Western Australia, Crawley, WA 6009, Australia
*to whom all correspondence should be addressed: lishancui63@126.com

Abstract:
This study investigated the effect of internal stress coupling on the deformation behavior of a NiTi matrix-Nb nanowire composite. It is found that residual internal stresses between the nanowires and matrix was created due to the mismatch between the elastic recovery strain of the Nb nanowires and the phase transformation strain of the NiTi matrix. These internal stresses affect the deformation behavior in subsequent deformation cycles, and the effect is dependent on the volume fraction of the nanowires.

Keywords: NiTi shape memory alloy, nanowire, composite, stress coupling effect

Introduction

To further enhance the functionalities and to expand the application of shape memory alloys and related smart materials, much effort have been given recently to develop hybrid shape memory materials, such as architectured shape memory alloys (SMAs) [1-3], functionally graded SMAs [4, 5] and shape memory composites [6]. These materials have the advantage to combine the unique functional properties of SMAs and those of the material structures. Some of these materials designs have shown remarkable and new properties, such as the extraordinary strength and low elastic modulus of NiTi-Nb nanowire composites [7], the "fish-tail" like shape change of compositionally graded NiTi strips[8], and the SMA honeycomb and cellulous structures [1-3]. Traditionally for a multi-constituent composite, the mechanical response to an external load is not only related to the intrinsic properties of each of the components, but also the interactions between them [9-12]. Such interactions are further complicated if one of the component is a conventional elastic-plastic metal and the other a phase transforming metal, such as SMAs.

Recently, our group reported a novel in situ NiTi-Nb nanowire composite. This composite is designed to harness the ultrahigh tensile strength and the large elastic strain of metallic nanowires via a mechanism of strain matching with the NiTi matrix. This composite material

has been shown to exhibit extraordinary mechanical properties including a high tensile yield strength of 1.65 GPa and a large elastic strain of 6.4% in "quasi-linear elasticity" with a low Young's modulus of 25.8 GPa [7]. The achievement of these extraordinary properties has been attributed to the interaction, or a unique strain matching, between the Nb nanowires and the NiTi matrix. The high strength of the Nb nanowires contributes to the overall load bearing capacity of the composite, whereas the stress-induced martensitic transformation of the NiTi matrix assures effective load transfer to the nanowires.

However, such composites composed of a phase-transforming matrix and an elastic nanowire reinforcement presents a new composite system, in terms of both its deformation mechanics and physical metallurgy, and much is to be understood of the microscopic mechanisms of stress and strain coupling between two components of drastically different characteristics. It is known that the recoverable strain of the martensitic transformation of the NiTi matrix is about 8% in tension [13]. The elastic strain limit of the embedded Nb nanowires is about 6% [7]. In addition, the stress-induced martensitic transformation of the NiTi matrix exhibits complete compliance (literally zero modulus of elasticity) during deformation whilst the Nb nanowires deform elastically following the Hooke's law. Understanding of the interactions, in particular the stress and strain coupling, between these components is of critical importance for the design and optimization of these composites. This paper presents a comparative study of the deformation behavior and microscopic mechanisms of two NiTi-Nb nanowire composites of different nanowire volume fractions.

Experimental procedure

Two ingots with nominal compositions of $Ti_{44}Ni_{47}Nb_9$ and $Ti_{39}Ni_{41}Nb_{20}$ were prepared by means of vacuum induction melting. The $Ti_{44}Ni_{47}Nb_9$ ingot (identified as NiTi-10Nb) contained 10 vol% lamellar Nb in NiTi matrix, and the $Ti_{39}Ni_{41}Nb_{20}$ ingot (identified as NiTi-20Nb) had 25 vol% lamellar Nb. The ingots were hot forged at 1123 K and then hot drawn to wires of 1.0 mm in diameter, and finally annealed at 1023 K for 1.2 ks. The NiTi-10Nb wire was then further cold drawn to 0.5 mm in diameter and the NiTi-20Nb wire was cold drawn to 0.55 mm in diameter. Samples used for tensile tests were cut from the wires, of 120 mm in length. The cut samples were given a final anneal in air at 748 K for 1.2 ks. Tensile tests were conducted on a MTS 810 servo-hydraulic material testing machine with a strain rate of 1×10^{-4} s^{-1} at room temperature. Microstructure of the samples was studied using a FEI Tecnai G20 high resolution transmission electron microscope (TEM). The TEM samples were first thinned to ~40 μm in thickness by grinding, followed by ion polishing to below 100 nm in thickness. The microstructure was analyzed using a commercial software from HREM Research Inc. as plug-in to "digital micrograph" (an image analysis software) developed by Gatan.

Results and discussion

Fig. 1 shows microstructure analysis of the NiTi-20Nb and NiTi-10Nb samples in annealed state. Figs. 1a and b are TEM bright field images of the NiTi-20Nb and NiTi-10Nb samples along the wire length direction, respectively. It is seen that long and continuous Nb nanowires, ranging from 30 nm to 50 nm in diameter, were all parallel-aligned in a nanocrystalline NiTi

matrix. The insets are the corresponding selected area electron diffraction patterns. The patterns are fully indexed to B2-NiTi and bcc-Nb. The bcc-Nb diffractions assemble highly broken rings and appear only at a few localized spots, implying strong wire texture of the Nb nanowires resulting from the severe drawing process [14]. The texture orientation is Nb[110] parallel to the wire axial direction. Fig. 1c is a high resolution electron micrograph of the matrix-nanowire interface. It is evident that the matrix and the embedded nanowire are well bonded at the atomic scale. Fig. 1d is a statistical analysis of the microstructure of the two alloy composites from 50 viewing areas, including NiTi grain size, Nb nanowire diameter and nanowire spacing. The average spacing between nanowires was calculated based on the volume fraction and average diameter of the nanowires. It is seen that average diameters of the Nb nanowires are practically identical in the two composites, whereas the average spacing between the Nb nanowires in NiTi-10Nb is nearly twice as large as that in NiTi-20Nb, apparently due to its lower volume fraction.

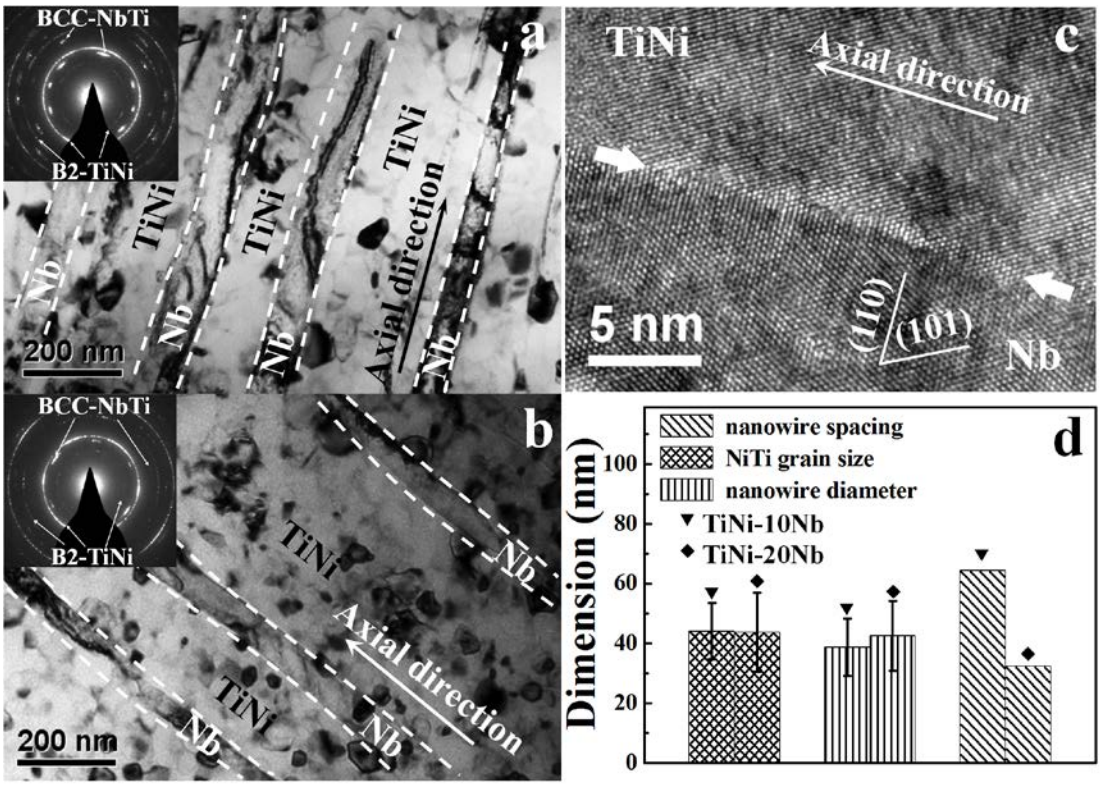

Figure 1. Transmission electron microscopic analysis of the NiTi-20Nb and TiNi-10Nb nanocomposites. a: TEM bright field micrograph of NiTi-20Nb and selected area electron diffraction pattern (inset). b: TEM bright field micrograph of NiTi-10Nb and selected electron diffraction pattern (inset). c: high resolution electron micrograph of a typical NiTi-Nb interface. d: statistical microstructure analysis of the two composites.

Fig. 2 shows tensile stress-strain curves of the two wire samples. Fig. 2a shows the tensile deformation behavior of NiTi-10Nb. The sample showed typical pseudoelastic behaviour, with a high upper stress plateau of 1100 MPa and a large stress hysteresis of 680 MPa in the first deformation cycle. The deformation behaviour is characteristic of localized deformation

[6], commonly referred to as the Lüders-type deformation [15, 16]. Fig. 2b shows the tensile deformation behavior of NiTi-20Nb. The sample showed an upper stress plateau at 1210 MPa upon the first loading, about 100 MPa higher than that of NiTi-10Nb. Upon unloading, the sample exhibited a two-stage pseudoelastic recovery. In subsequent deformation cycles, the sample quickly evolved into a uniform deformation behavior with a continuously increasing stress over a large stress window during the stress-induced martensitic transformation.

It is seen that the two samples showed quite distinctive deformation beahviour, and behaviour evolution during mechanical cycling, despite the similar composite structures of the two samples. This is attributed to the different volume fractions of the Nb nanowires in the two composites. The interactions between the Nb nanowires and the NiTi matrix may be explained as following.

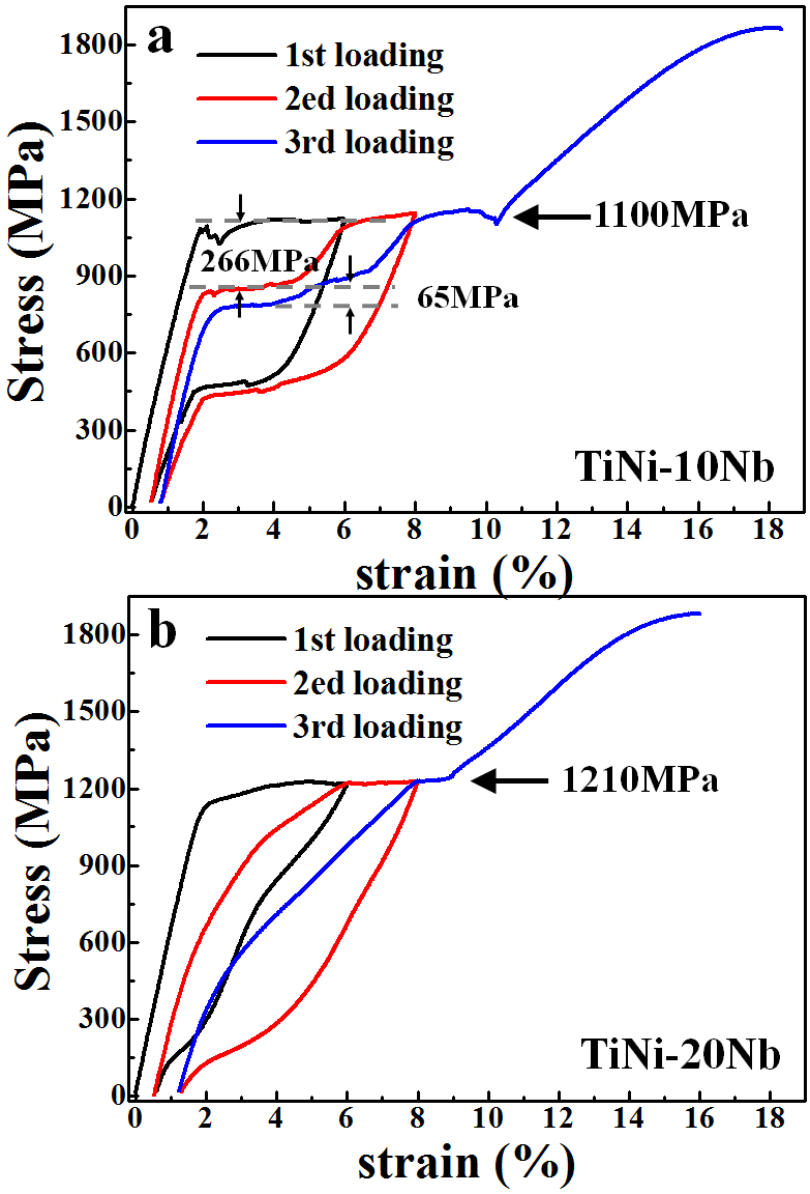

Figure 2. Tensile stress-strain curves of the composite wires. a: NiTi-10Nb. b: NiTi-20Nb.

For the first tensile cycle, the stress induced transformation of the NiTi matrix is the same as that of a polycrystalline NiTi, and proceeds in a Lüders-type manner. The effect of the embedded Nb nanowires on deformation of the composite is that, at the time when stress-induced martensite transformation takes place in NiTi matrix, the applied stress also loads the embedded nanowire to a considerable elastic strain, matching the transformation strain of the NiTi matrix locally [7]. Therefore, a higher content of nanowires in NiTi-20Nb merely leads to a higher stress plateau than that of NiTi-10Nb and both samples exhibited Lüders-type deformation upon the first loading. After the completion of the first tensile deformation cycle, internal stresses are expected to develop as a consequence of the mismatch in magnitude of the elastic recovery strain of the Nb nanowires and the shape memory strain of the NiTi matrix. It has been shown previously by X-ray diffraction that the Nb nanowires in a similar composite developed a compressive residual strain after a tensile deformation to 9.5% [6, 7]. Correspondingly, an internal tensile stress is creased in the NiTi matrix. These internal stresses are expected to influence the stress induced martensite transformation of the composites in subsequent deformation cycles.

This concept is schematically illustrated in Fig. 3. Fig. 3a indicates the original state of the composite. Upon the first tension to 8.0%, the NiTi matrix deforms via stress-induced martensitic transformation in a Lüders-type manner over a stress plateau [15, 17], whilst the Nb nanowires deform first elastically and then plastically after passing the elastic strain limit. It is known that the elastic strain limit of the Nb nanowires is smaller than that of the shape memory strain of NiTi [18, 19]. Upon unloading, the NiTi matrix transforms back to austenite and in doing so recovers to its original length. The Nb nanowires, on the other hand, have experienced plastic deformation and are only able to recover the elastic component of the total elongation, thus impede the full recovery of the NiTi matrix. This leads to the creation of internal stresses in both the nanowires and the matrix after the first tensile cycle. Internal stress distribution in the matrix is schematically shown in Fig. 3b. The stress is the highest at near the NiTi-Nb interface and decays rapidly with increasing distance from the nanowire, creating a narrow “stress-affected zone” around the nanowires. The NiTi-10Nb composite has larger inter-nanowire spacing, thus the majority of the NiTi matrix is in the “unaffected zone”. During subsequent deformation cycles, the stress induced martensitic transformation proceeds via Lüders-type localized manner, as in the first cycle. The NiTi-20Nb composite, however, has much smaller inter-nanowire spacing, and the majority of the NiTi matrix is under the influence of the gradient internal stress. Under such condition, the critical applied stress required to induce the martensitic transformation increases progressively with increasing distance from the nanowires when the internal stress decreases, leading to a progressively increasing applied stress during the course of the transformation.

To verify this mechanism, HRTEM examinations were conducted on samples taken from different sections of a 6% strained NiTi-10Nb wire. Internal strain distribution was studied by means of geometric phase analysis (GPA) of HRTEM micrographs. GPA is a method of quantitative analysis of relative distortion of HRTEM images by establishing relationship between displacements and the geometric phase of corresponding lattice fringes [20]. Under

the condition of comma free alignment and the electron beam interacting with a centrosymmetric structure, for example the B2-NiTi matrix and the Nb nanowire, the position of lattice fringe may be regarded a good approximation to positions of atomic planes thus allowing displacement field in real space to be honestly imaged by lens[21]. This method has been used to measure lattice strains in several different material systems [22-24].

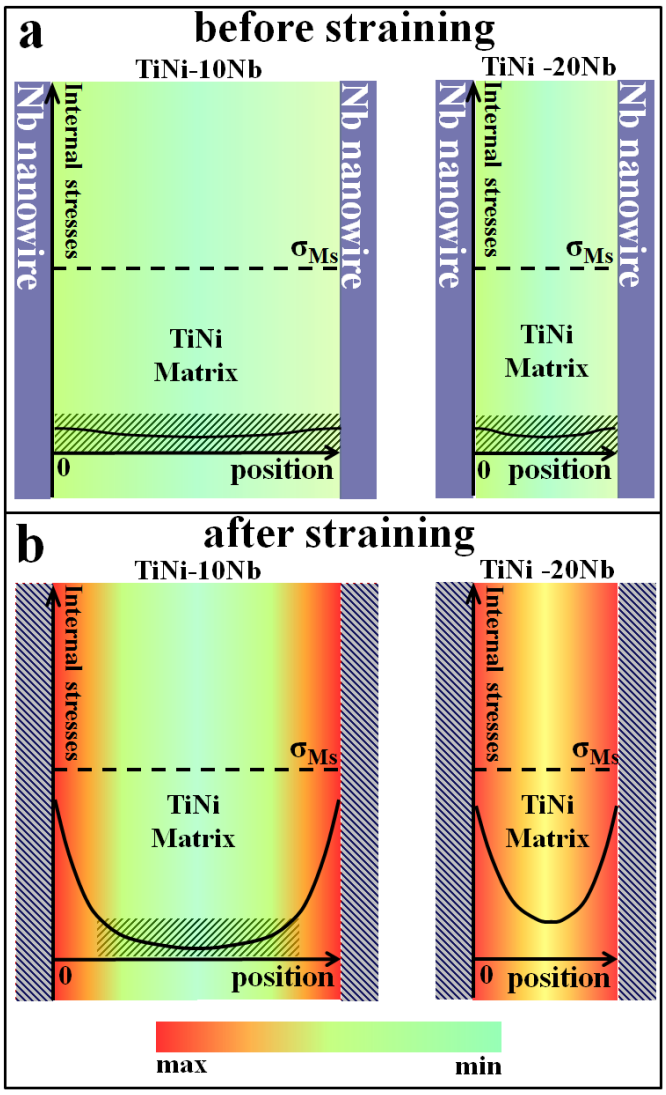

Figure 3. Schematic of internal stress fields distribution evolution of NiTi-Nb composites with different volume fractions of nanowires.

Fig. 4 shows HRTEM micrographs, all of the longitudinal view of the composite wire, and corresponding GPA analysis. Fig. 4a is taken from a sample inside a Lüders band and the NiTi grain is adjacent to a Nb nanowire. The incident beam was parallel to the $[\bar{1}11]$ axis of the Nb nanowire, as determined from the FFT pattern shown in the inset. The arrow in the inset indicates the $\boldsymbol{g}$ vector used for fringe deformation analysis. Fig 4b is the fringe deformation map of the NiTi grain in Fig. 4a. Fig. 4c is the lattice strain profile of fringe deformation corresponding to the marked area shown in Fig. 4b. The arrow in the marked

box in b corresponds to the arrow under the profile in c. It is seen that the lattice strain of the grain on the side adjacent to the Nb nanowire is 2.8% higher than that on the far side. A sharp strain gradient was also observed within a range of about 15 nanometers. Fig. 4d and e are the HRTEM image and corresponding fringe deformation map of another NiTi grain and its neighboring nanowire. This sample was taken in an area outside the Lüders band. Fluctuations in fringe deformation are shown in the insets of Fig. 4e. The strain variation is ~0.5%. Fig. 4f and g are the HRTEM analysis of another NiTi grain within the Lüders band, which is far away from Nb nanowires and is surrounded by NiTi grains only. It is seen from the insets in Fig. 4g that variations of lattice strains across the grain are no larger than ±0.8%, similar in magnitude to those in the grain shown in Fig. 4e. The above analysis demonstrates that after deformation the NiTi matrix adjacent to nanowires is subjected to high internal stresses whereas the NiTi regions far from the nanowires are much less affected.

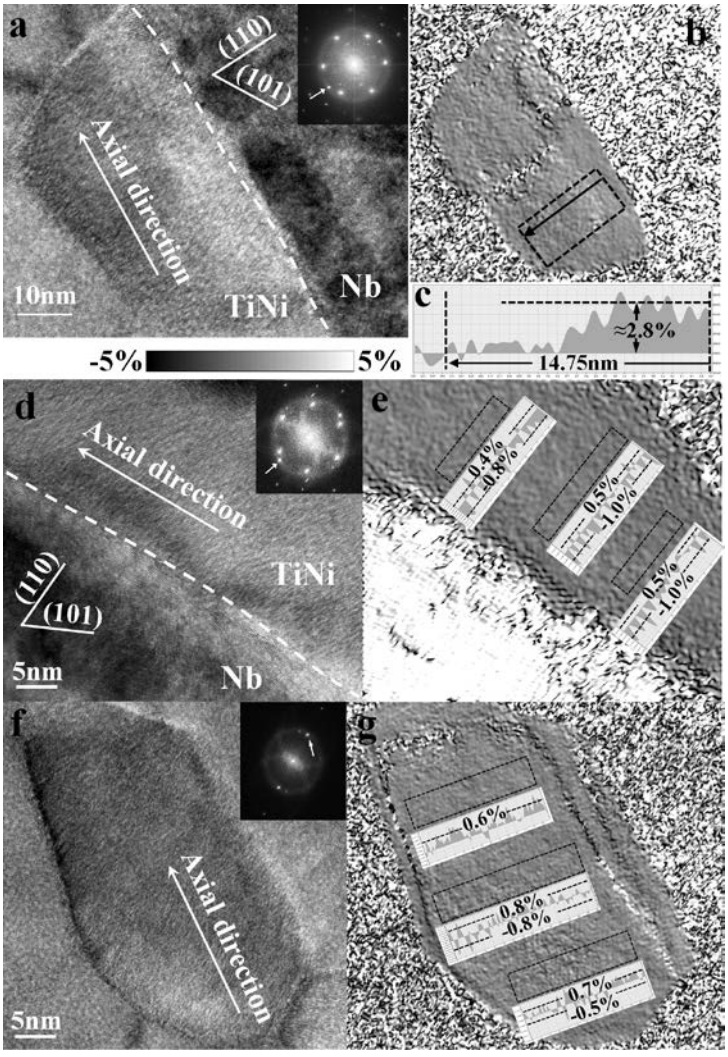

Figure 4 TEM and GPA analysis of strain in NiTi grains at different locations. HRTEM image and fringe deformation analysis of, a to c: typical NiTi grain inside Lüders band of 6% strained sample and neighboring a nanowire; d and e: typical NiTi grain in annealed state and neighboring a nanowire; f and g: typical NiTi grain inside Lüders band of 6% strained sample and surrounded by NiTi only.

Conclusions

To summarize, the composite system composed of a phase-transforming matrix and aligned elastic nanowire reinforcements presents a new micromechanical system. Due to the mismatch in recoverable strains of the NiTi matrix and Nb nanowires, coupled internal stresses were created between the nanowire and the matrix after tensile deformation. The internal stress affected zone in the matrix is limited in a small range around the nanowires. These stresses affect the stress-induced martensitic transformation behavior of the NiTi in the zones. The macroscopic deformation behavior of the composite is influenced by the volume fraction of the nanowires and can be tailored by applying different amount of the pre-deformation. This understanding enables us to design and engineer specific properties of NiTi-nanowire based superelastic composites.

Acknowledgement

This work is supported by the key program project of National Natural Science Foundation of China (NSFC) (51231008), Australian Research Council (Grant No. DP140103805), the National Natural Science Foundation of China (NSFC) (Grant Nos. 51001119) and the Key Project of Chinese Ministry of Education (313055).

References

[1] A.S. John, S.G. David, F. John, Smart Materials and Structures, 16 (2007) S170.

[2] V. Favier, J.Y. Cavaille, G.R. Canova, S.C. Shrivastava, Polymer Engineering & Science, 37 (1997) 1732-1739.

[3] V. Favier, H. Chanzy, J. Cavaille, Macromolecules, 28 (1995) 6365-6367.

[4] H. Nakayama, K. Tsuchiya, M. Umemoto, Scripta Materialia, 44 (2001) 1781-1785.

[5] S.S. Bashir, L. Yinong, R. Gerard, Smart Materials and Structures, 22 (2013) 025030.

[6] S. Hao, L. Cui, D. Jiang, Y. Wang, X. Shi, J. Jiang, D.E. Brown, Y. Ren, Applied Physics Letters, 101 (2012) 173115-173115-173113.

[7] S. Hao, L. Cui, D. Jiang, X. Han, Y. Ren, J. Jiang, Y. Liu, Z. Liu, S. Mao, Y. Wang, Y. Li, X. Ren, X. Ding, S. Wang, C. Yu, X. Shi, M. Du, F. Yang, Y. Zheng, Z. Zhang, X. Li, D.E. Brown, J. Li, Science, 339 (2013) 1191-1194.

[8] Q. Meng, H. Yang, Y. Liu, T.-h. Nam, Scripta Materialia, 67 (2012) 305-308.

[9] P.J. Withers, W.M. Stobbs, O.B. Pedersen, Acta Metallurgica, 37 (1989) 3061-3084.

[10] K. Johansen, H. Voggenreiter, G. Eggeler, Materials Science and Engineering: A, 273–275 (1999) 410-414.

[11] M. Kawai, International Journal of Plasticity, 16 (2000) 263-282.

[12] Y. Li, L. Cui, Y. Zheng, D. Yang, Materials Letters, 51 (2001) 73-77.

[13] P. Sittner, Y. Liu, V. Novak, Journal of the Mechanics and Physics of Solids, 53 (2005) 1719-1746.

[14] V. Vidal, L. Thilly, S. Vanpetegem, U. Stuhr, F. Lecouturier, P. Renault, H. Vanswygenhoven, Scripta Materialia, 60 (2009) 171-174.

[15] G. Tan, Y. Liu, P. Sittner, M. Saunders, Scripta Materialia, 50 (2004) 193-198.

[16] Y. Liu, Y. Liu, J. Van Humbeeck, Scripta materialia, 39 (1998) 1047-1055.

[17] Y. Liu, Y. Liu, J. Humbeeck, Scripta Materialia, 39 (1998) 1047-1055.

[18] X. Zhang, H. Sehitoglu, Materials Science and Engineering A, 374 (2004) 292-302.

[19] X. Huang, G.J. Ackland, K.M. Rabe, Nature Materials, 2 (2003) 307-311.

[20] E. Snoeck, B. Warot, H. Ardhuin, A. Rocher, M.J. Casanove, R. Kilaas, M.J. Hytch, Thin Solid Films, 319 (1998) 157-162.

[21] M.J. Hÿtch, Scanning Microscopy, 11 (1997) 53-66.

[22] C.R.M. Afonso, P.L. Ferrandini, A.J. Ramirez, R. Caram, Acta Biomaterialia, 6 (2010) 1625-1629.

[23] J. Chung, L. Rabenberg, Ultramicroscopy, 108 (2008) 1595-1602.

[24] M. Hytch, F. Houdellier, Microelectronic Engineering, 84 (2007) 460-463.